RACORO EXTENDED-TERM AIRCRAFT OBSERVATIONS OF BOUNDARY LAYER CLOUDS

BY ANDREW M. VOGELMANN, GREG M. MCFARQUHAR, JOHN A. OGREN, DAVID D. TURNER, JENNIFER M. COMSTOCK, GRAHAM FEINGOLD, CHARLES N. LONG, HAFLIDI H. JONSSON, ANTHONY BUCHOLTZ, DON R. COLLINS, GLENN S. DISKIN, HERMANN GERBER, R. PAUL LAWSON, ROY K. WOODS, ELISABETH ANDREWS, HEE-JUNG YANG, J. CHRISTINE CHIU, DANIEL HARTSOCK, JOHN M. HUBBE, CHAOMEI LO, ALEXANDER MARSHAK, JUSTIN W. MONROE, SALLY A. MCFARLANE, BEAT SCHMID, JASON M. TOMLINSON, AND TAMI TOTO

A campaign involving 260 flight hours over more than 5 months provides the first extended-term aircraft dataset of a wide range of continental boundary layer clouds, and aerosol properties for climate studies.

Shallow boundary layer clouds are ubiquitous over many parts of the globe and strongly influence Earth's radiative energy balance (Hartmann et al. 1992). However, our understanding of these clouds is insufficient to solve pressing scientific problems. Cloud feedback represents the largest uncertainty among all climate feedbacks in general circulation models (GCMs), and subtropical boundary layer clouds are the dominant contributor to this uncertainty (Bony and Dufresne 2005; Williams and Tselioudis 2007; IPCC 2007). Shallow cumulus convection over land is affected by land surface heterogeneity (e.g., Weaver and Avissar 2001) and is typically stronger and more time varying than over ocean (Brown et al. 2002). It regulates the surface radiation budget and contributes to the

AFFILIATIONS: VOGELMANN AND TOTO—Brookhaven National Laboratory, Upton, New York; MCFARQUHAR AND YANG—University of Illinois at Urbana–Champaign, Urbana, Illinois; OGREN AND FEINGOLD—NOAA/Earth System Research Laboratory, Boulder, Colorado; TURNER—NOAA/National Severe Storms Laboratory, Norman, Oklahoma, and University of Wisconsin—Madison, Madison, Wisconsin; COMSTOCK, LONG, HUBBE, LO, MCFARLANE, SCHMID, AND TOMLINSON—Pacific Northwest National Laboratory, Richland, Washington; JONSSON AND WOODS—Naval Postgraduate School, Monterey, California; BUCHOLTZ—Naval Research Laboratory, Monterey, California; COLLINS—Texas A&M University, College Station, Texas; DISKIN—NASA Langley Research Center, Hampton, Virginia; GERBER—Gerber Scientific, Inc., Reston, Virginia; LAWSON—SPEC Inc., Boulder, Colorado; ANDREWS—NOAA/Earth System Research Laboratory, Boulder, Colorado, and University of Colorado, Boulder, Colorado; CHIU—University of Reading, Reading, Berkshire, United Kingdom; HARTSOCK AND MONROE—Cooperative Institute for Mesoscale Meteorological Studies, University of Oklahoma, Norman, Oklahoma; MARSHAK—NASA Goddard Space Flight Center, Greenbelt, Maryland
CORRESPONDING AUTHOR: Andrew Vogelmann, Brookhaven National Laboratory, Bldg. 490D, Upton, NY 11973
E-mail: vogelmann@bnl.gov

The abstract for this article can be found in this issue, following the table of contents.

DOI:10.1175/BAMS-D-11-00189.1

In final form 22 December 2011

preconditioning of deeper convection (Chaboureau et al. 2004; Khairoutdinov and Randall 2006; Rio et al. 2009). However, GCMs misrepresent the diurnal cycle of continental convection, with rain onset typically occurring too early (Betts and Jakob 2002).

Several issues complicate understanding boundary layer clouds and simulating them in GCMs and numerical weather prediction models. Boundary layer clouds include stratus, stratocumulus, and cumulus, which can be tenuous and/or occur in partly cloudy skies. Cumulus cloud size distributions typically follow a negative power-law function (e.g., Cahalan and Joseph 1989), where increasingly larger numbers of small clouds are present down to the satellite sensor's detection limit (on the order of 10 m). The high spatial variability of these clouds poses an enormous computational challenge, because their horizontal dimensions (e.g., McFarquhar et al. 2004) and internal variability (e.g., Marshak et al. 1998) occur at spatial scales much finer than the computational grids used in GCMs (order 100 km). Because convection is not resolved by GCMs, it must be parameterized. However, model-parameterized boundary layer clouds do not agree well with observations because small-scale turbulence and convection are not properly represented (e.g., Lenderink et al. 2004) and GCMs typically underestimate the occurrence of low-level clouds at all latitudes (Zhang et al. 2005).

Aerosol–cloud interactions further complicate boundary layer cloud measurement and simulation. An increase in aerosol causes an increase in droplet concentration and a decrease in droplet size [for a fixed liquid water content (LWC)], which enhances cloud albedo (Twomey 1974). This aerosol effect on cloud albedo is the climate forcing mechanism with the greatest uncertainty (IPCC 2007). Additionally, the aerosol influences processes such as precipitation and cloud lifetime (Albrecht 1989) and induce dynamical responses such as changes in cloud thickness (Pincus and Baker 1994; Boers and Mitchell 1994). The covariance of cloud liquid water and aerosol within the boundary layer complicates isolation of the albedo enhancement due to aerosol from meteorological factors, although progress is being made (e.g., McComiskey et al. 2009; Berg et al. 2011). An added complication is that at small scales (on the order of meters to tens of meters) distinguishing cloud from aerosol is increasingly difficult, due to the effects of aerosol humidification (Charlson et al. 2007), cloud fragments (Koren et al. 2007), and photon scattering between clouds (Wen et al. 2007).

The high spatial variability of boundary layer clouds complicates the use of surface and satellite remote sensing to characterize cloud properties (Turner et al. 2007b), which interferes with the acquisition of the long-term statistics needed to evaluate parameterizations. For example, the small sizes of cumuli mean that most conventional satellite sensors [e.g., Moderate Resolution Imaging Spectrometer (MODIS)] are not be able to retrieve their properties given the satellite resolution (e.g., Dey et al. 2008); moreover, if retrieved, cumulus cloud droplet size and optical depth are usually biased (e.g., Marshak et al. 2006). Further, these clouds commonly have liquid water paths (LWPs) less than 100 g m^{-2}, which are referred to as Clouds with Low Optical Water Depths (CLOWD; Turner et al. 2007b). At the Atmospheric Radiation Measurement (ARM; Ackerman and Stokes 2003) program sites, from the tropics to the Arctic, 50% or more of the liquid water–bearing clouds have LWPs below this value (Turner et al. 2007a). However, CLOWD systems challenge the limits of remote sensing techniques. For example, LWPs retrieved by 18 state-of-the-art retrieval algorithms differed by 50%–100% for a simple, warm stratiform cloud (Turner et al. 2007b). These differences are unacceptably large, especially when Earth's radiative energy balance is particularly sensitive to small perturbations in LWP when LWP is small (Sengupta et al. 2003; Turner et al. 2007b).

Experimental goals. The need for a better understanding of boundary layer clouds can only be achieved by acquiring high-quality in situ data that can be applied to process studies, finescale model evaluation, and the refinement of retrieval algorithms. A first-of-a-kind cloud aircraft campaign was conducted to obtain an extended-term, statistical characterization of continental, boundary layer, liquid water clouds. Coordinated by the ARM Aerial Facility (AAF), the Routine AAF CLOWD Optical Radiative Observations (RACORO) campaign operated for five months, from 22 January to 30 June 2009, over the Southern Great Plains (SGP) ARM Climate Research Facility (ACRF) in Lamont, Oklahoma. This location is well situated because boundary layer clouds frequently occur there during these months (Lazarus et al. 2000) offering the potential for good statistics, and the SGP's extensive complement of surface measurements provides ancillary data that support modeling studies and enable evaluation of a variety of surface retrieval algorithms.

During RACORO, the Center for Interdisciplinary Remotely-Piloted Aircraft Studies (CIRPAS) Twin Otter made comprehensive measurements of cloud, aerosol, radiation, and atmospheric state

parameters. RACORO's long duration enabled sampling of a range of environmental conditions associated with the seasonal transition from winter to summer. RACORO aimed to obtain an unbiased characterization of the cloud-field properties, namely a representative sample of the clouds present, not of a few visually appealing clouds that were atypical of the cloud population. This provides researchers with a comprehensive dataset to address the science objectives listed in Table 1.

This type of long-term program is a next step for aircraft campaigns, made possible by the instrumental expertise developed over the last couple of decades, where the continued enhancement of in situ instruments and their postprocessing algorithms has made them suitable for routine observations (McFarquhar et al. 2011). This is analogous to how the establishment of routine ground-based retrieval programs (e.g., ARM or CloudNet; Illingworth et al. 2007) followed the accomplishment of short-term, ground-based deployments. However, new approaches involve new challenges. In this paper, challenges in the conduct of a long-term, in situ cloud-sampling program and their solutions are described, followed by preliminary results of the types of scientific questions that are enabled by RACORO data.

ROUTINE SAMPLING: A NEW CLOUD-SAMPLING PARADIGM. Long-term aircraft sampling requires a simplified operating paradigm that is different from typical, short-term, intensive aircraft field programs. Such challenges were first negotiated by the ARM In-situ Aerosol Profiling (IAP) Program, which made aircraft observations of aerosol properties in cloud-free skies over the SGP for seven years, averaging two flights per week (Andrews et al. 2004). RACORO adopted the IAP Program's practice of simplification for operations and instrument selection and negotiated issues particular to cloud sampling, such as the more extensive payload and timing the flights to coincide with relevant cloud conditions.

Instrument selection. Any instrument requires maintenance, calibration, and resources to ensure data quality and archive the data. To enable cost-effective routine observations, instruments need a track record of reliability and minimal maintenance requirements and must provide raw data that can be easily processed into its final form. Newer or experimental instruments, which could have been desirable for RACORO, were not used if they required more attention than was possible for a long-term campaign. Additionally, instruments with small weight and low power consumption were

Table 1. RACORO scientific objectives and steps to achieve them (for a list of science questions related to these objectives, see the science and operations plan at www.arm.gov/publications/programdocs/doe-sc-arm-0806.pdf?id=60).

1) Improve cloud simulations in climate models
Meteorological state was measured by aircraft and surface instrumentation, which provides critical information on moisture availability and updraft intensity at cloud base. These data facilitate examining how meteorological factors influence cloud dynamics, cloud properties, and aerosol–cloud interactions. The collection of statistics and their seasonal variations provide constraints and probability density functions (PDFs) of many variables that can be used to evaluate and improve climate model simulations of these clouds.
2) Investigate aerosol–cloud interactions
RACORO observed physical aerosol properties associated with cloud variability, such as aerosol amount, aerosol size distribution, and the number of cloud condensation nuclei (CCN). These data enable addressing the problem of deciphering how the aerosol affects cloud properties. This attribution is confounded by the meteorological variability that requires RACORO-type, long-term statistics to resolve.
3) Investigate cloud radiative forcing
Radiometric observations made by the aircraft, in addition to in situ cloud microphysical observations, can be used to characterize the high spatial variability of these cloud systems and their radiative impacts. Below-cloud narrowband radiometer measurements can be used to retrieve cloud properties and obtain a map of the cloud field optical properties needed to assess the impact of the cloud field on Earth's radiative energy budget.
4) Evaluate remotely sensed cloud properties
The radiometric observations made by surface instruments and on satellites are used to retrieve cloud liquid water amount and cloud drop size, which are essential for cloud and climate studies. However, large differences exist between different state-of-the-art retrievals of boundary layer clouds, and Earth's radiative energy balance can be very sensitive to small changes in their properties. RACORO observations can help evaluate these retrievals.

emphasized to enable the use of a smaller and less expensive aircraft.

Because boundary layer clouds vary rapidly over short horizontal distances, slow aircraft speed, fast instrument response times, and large particle sampling volumes were also needed. Tradeoffs were inevitable when balancing the need for fast sampling rates against the cost and quality of the measurement. Because instruments measuring exactly what was needed did not always fit the reliability and cost constraints, whenever possible a pair of robust instruments was deployed, with a slower measurement providing the needed accuracy and a faster measurement quantifying the variability. Redundancy of critical parameters was also stressed to ensure data continuity because it was uncertain a priori which instruments would prove reliable over the course of the long-term campaign.

The CIRPAS Twin Otter had the desired power and speed (50 m s^{-1}). It also already had an extensive set of cross-disciplinary instruments, well tested in many prior field campaigns, that was augmented with guest instruments. The comprehensive, multidisciplinary suite of instruments flown is

Table 2. RACORO multidisciplinary payload. Instrumentation listing is grouped by category given on the left. Radiometer viewing direction is indicated by ↑ (upward looking) and ↓ (downward looking). The last column indicates whether the measurement is relatively slow (S) or fast (F; usually 1 Hz or better). Brackets indicate paired measurements, where the faster measurements may help interpret the slower-response measurements (see text). For the dual-column CCN spectrometer (S/F), one column was fixed at 0.2% supersaturation (SS) and sampled at 1 Hz while the second column scanned through a range of SSs (0.2%, 0.28%, 0.4%, 0.57%, and 0.8%) in about 25 min.

	Measurement	Instrument	Speed
Cloud microphysics	LWC	Particle Volume Monitor-100A (Gerber Probe)	F
		Science Engineering Associates, Inc. (SEA) LWC probe (WCM-2000, LWC only)	F
	Drop size distribution	Forward Scattering Spectrometer Probe-100 (FSSP)	F
		Cloud and Aerosol Spectrometer (CAS)	F
		1D Cloud Imaging Probe (CIP)	F
		2D CIP	F
		2D Stereo Probe (2D-S)	F
	Cloud extinction	Cloud Integrating Nephelometer (CIN)	F
Radiation	Broadband irradiances	↑↓ shortwave Kipp & Zonen (a modified CM22)	S
		↑ Sunshine Pyranometer (SPN1)	F
		↑↓ longwave Kipp & Zonen (a modified CG4)	S
	Spectral radiances	↑↓ Infrared Thermometer (IRT)	F
		↑ or ↓ HydroRad-3 hyperspectral radiometer	F
	Spectral irradiances	↑↓ Multifilter Radiometer (MFR)	F
		↑↓ HydroRad-3 hyperspectral radiometer	F
Aerosol	CCN	Dual-column CCN spectrometer	S/F
	Size distribution	Differential Mobility Analyzer (DMA)	S
		Two condensation nuclei particle counters (CPCs)	F
		Ultrafine CPC (UFCPC)	F
		Passive Cavity Aerosol Spectrometer Probe (PCASP)	F
Atmospheric state	Temperature	Rosemount (primary) and Vaisala (backup)	F
	Water vapor	Two chilled-mirror hygrometers (EdgeTech, CR2)	S
		Diode Laser Hygrometer (DLH)	F
	Horizontal winds and updraft velocity	Determined from multiple aircraft sensors	F
	Conditions	Handheld photos	S
		DAQ flight images/video	F

listed in Table 2. Highlights of the measurements include the following:

- Cloud microphysics observations: multiple measures of cloud liquid water content and of drop size distribution spanning the range of cloud particle diameters (i.e., 0.5–1,600 μm);
- Aerosol observations: total number concentration, size distribution, and cloud condensation nuclei (CCN) concentration needed for studies of aerosol–cloud interactions;
- Radiative observations: broadband solar and thermal irradiances for energy budget analyses and high-resolution spectral irradiances and radiances for retrieving cloud properties; and
- Atmospheric state observations: turbulence, temperature, and water vapor concentration, including an ultra-fast measurement of water vapor (100 Hz) to capture gradients in and around clouds.

Operations: A yeoman's effort. Short-term, intensive field campaigns normally have many personnel on site attending to the operations, measurements, and science for their duration. However, to keep RACORO cost effective, only a skeleton crew was present for most of the program, with occasional visits by aircraft maintenance personnel, instrument principal investigators (PIs), and researchers. The diverse measurement payload was operated by eight onboard computers, with only one person initializing the computers prior to takeoff, monitoring the data during flight, and archiving the raw data after flight completion. This is why only critical and robust instruments were chosen, because troubleshooting could strain the already-busy personnel.

The on-site personnel were rotated as much as possible. The rest of the team participated remotely via telecons in flight decisions and planning. For example, the seven-member RACORO steering committee worked as science PIs in pairs for two-week shifts during the campaign. Their shifts were staggered by a week so that the member joining the rotation could spin up on operations and weather conditions and then maintain continuity when the rotation progressed the next week. The whole team participated in a weekly telecon to discuss progress to date, instrument status, and to plan any needed adjustments.

For the last month, the RACORO flights were coordinated with flights made by the National Aeronautics and Space Administration (NASA) King Air aircraft, which carried the high-spectral-resolution lidar (Hair et al. 2008) and the research scanning polarimeter (Cairns et al. 2009). The overlapping data from the King Air complement the five-month RACORO dataset and are an example of how a short-term deployment can complement the objectives of a long-term deployment by bringing more sophisticated but more manually intensive instruments to the field for a period.

OUTCOME AND PRELIMINARY RESULTS.

Campaign overview: Sampling seasonal variation. During the five-month campaign, the CIRPAS Twin Otter logged 260 research hours during 59 flights. Overall, the instrument complement worked well, especially for such a long, challenging campaign. On the occasion that an instrument issue arose, the measurement of the parameter usually had coverage via instrument redundancy.

The winter-to-summer transition experienced during this period is illustrated in Fig. 1 by profiles of temperature and specific humidity over the SGP (the target site), which show the atmosphere's evolution from a colder and drier state to a warmer and moister state. At the start of the campaign, the SGP region experienced dry conditions associated with a La Niña–like pattern that began in fall 2008 and carried through the winter into March 2009. During this period, the region was several degrees warmer than average with 20%–40% of the average precipitation. The lack of moisture resulted in fewer cloudy days at the start of RACORO than expected, but by spring conditions transitioned to a more typical moisture pattern that provided some of the best cloud cases during the last months of the campaign.

When boundary layer clouds were absent, the multidisciplinary payload was used to characterize the broader environment during "noncloud flights." These flights included an extensive characterization of aerosol size distributions and CCN concentrations, mapping the highly variable surface albedo, characterizing the structure of the boundary layer turbulence, and characterizing the response of upward-looking shortwave radiometers to aircraft attitude. Of the 59 flights, 33 involved cloud-sampling missions. The primary objective(s) of each RACORO flight is given in Fig. 1c, and the number of flight hours dedicated to each objective is summarized in Fig. 2.

The long-term nature of RACORO enabled the sampling of boundary layer clouds under a variety of environmental and aerosol conditions. Figure 3 summarizes the ranges of three parameters that are critical to cloud formation, sampled on each flight:

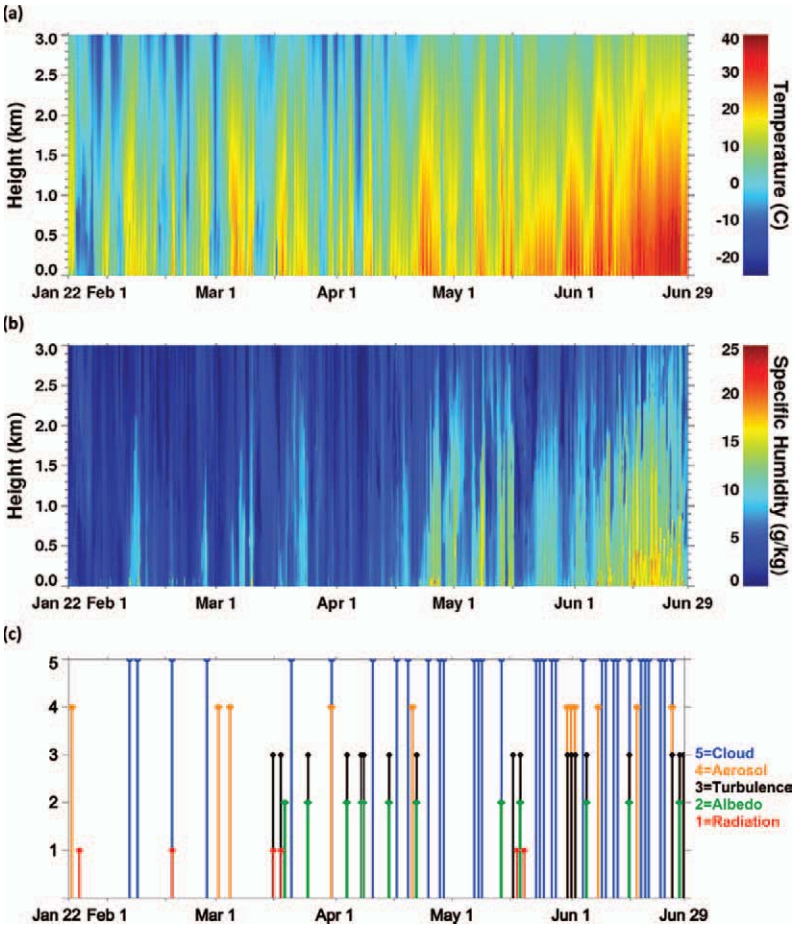

Fig. 1. Overview of SGP atmospheric conditions during RACORO and flight types. Atmospheric profiles at the SGP during RACORO are given for (a) temperature and (b) specific humidity, obtained from the continuous profiles available from the Merged Sounding value-added product (www.arm.gov/publications/tech_reports/doe-sc-arm-tr-087.pdf). Profiles illustrate the strong seasonal transition from the colder, drier wintertime air to warmer, moister summertime air. (c) The occurrence of RACORO flights, with the primary flight type/mission indicated by the legend. Overlapping lines indicate multiobjective flights.

water vapor mixing ratio, relative humidity (RH), and CCN concentration. Approximately two-thirds of the clouds flights (colored blue) occurred in May and June. Although more sampling during the earlier months would have been preferred, the cloud flights span the ranges present within the overall record. This suggests that clouds were sampled under a range of environmental states representative of those associated with the seasonal transition.

The clouds sampled. A full range of boundary layer cloud types was sampled (i.e., stratus, stratocumulus, cumulus, and combinations thereof) as summarized in Fig. 4. (For a description of the cloud flight decision-making process, see the "Where and when to fly" sidebar.) Broken cloud types were frequently sampled, with 77% of the cloud flights occurring in cumulus and stratocumulus. Figure 5 shows that the stratocumulus cases tended to occur toward the beginning of the campaign and the cumulus cases started to appear by early May. The total amount of in-cloud sampling was 11 h, where in-cloud is defined as LWC > 0.01 g m^{-3}. The ranges of LWC sampled are consistent with those of fair-weather

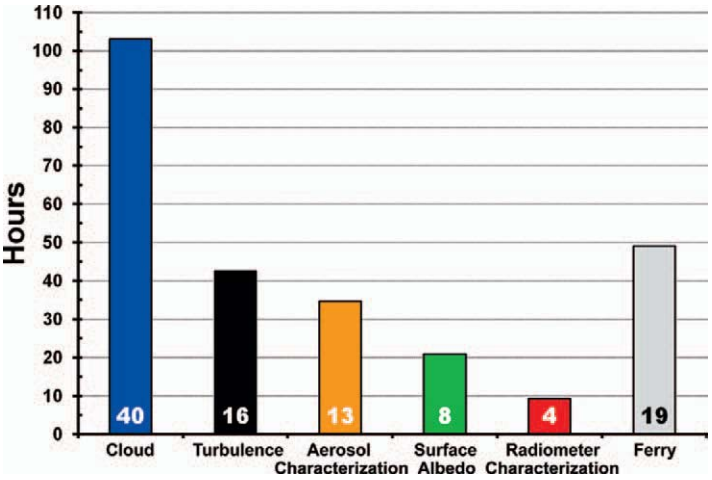

Fig. 2. RACORO flight hour distributions per objective. Total flight hours are plotted per primary objective: cloud sampling, boundary layer turbulence characterization, aerosol characterization, surface albedo mapping, and radiometer tilt-correction characterization. The ferry time to and from the study site is provided, which also was used to scout the conditions in preparation for the on-site patterns (e.g., determine cloud altitudes, boundary layer height, and wind direction). The primary objective dictated the flight pattern used; however, a given flight pattern could serve the sampling needs of other objectives. At the base of each bar, the time is expressed as a percentage of the total 260 h flown.

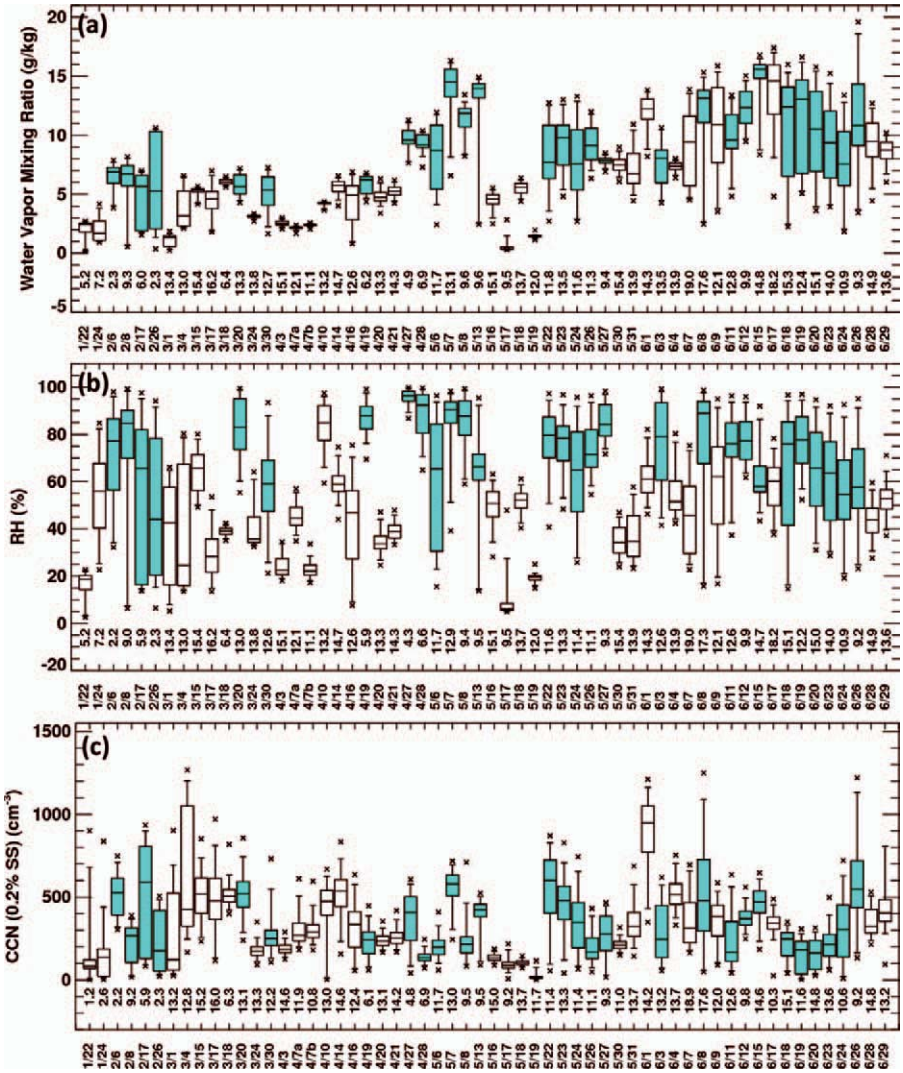

Fig. 3. Overview of conditions sampled during RACORO flights. Overall, the flights captured a wide range of environmental conditions, as illustrated by the on-station values given as a function of flight date for (a) water vapor mixing ratio, (b) RH, and (c) CCN at 0.2% SS. Water vapor mixing ratio and RH are determined from the Rosemount temperature and the EdgeTech chilled-mirror hygrometer measurements. Blue shading indicates a cloud flight. For consistency between the cloud and noncloud flights, all values are screened for cloud-free conditions (CAS LWC < 0.01 g m^{-3}). The percentiles depicted in the box-and-whisker plots are as follows: 5th, 25th, 50th, 75th, and 95th. The x's at the ends of the box and whisker represent the 2nd and 98th percentiles. The number below each box and whisker is the number of 1-Hz samples in thousands. One flight (24 Apr) is not plotted because it had data-transfer issues.

boundary layer clouds (e.g., Miles et al. 2000), where the per-flight median values ranged from about 0.05–0.15 g m^{-3} and the 75th percentiles reached almost 0.4 g m^{-3} (Fig. 5). The median in-cloud updrafts (not shown) were typically 0.25–1.4 m s^{-1}, representative of velocities associated with shallow clouds, and the 75th percentiles were 0.3–2.8 m s^{-1}. Note that the cloud statistics are applicable only to warm clouds, because flight safety regulations prohibited in-cloud operation under freezing conditions (temperature ≤0°C).

These aircraft measurements are placed in a broader context using cloud LWPs retrieved from the SGP's microwave radiometer (MWR) when the Twin Otter was aloft. Figure 6 shows that RACORO primarily sampled CLOWD-type systems, with almost 80% of the cumulative frequency distribution of LWP being below 100 g m^{-2}. Figure 6 also indicates the challenge in observing boundary layer cloud LWP

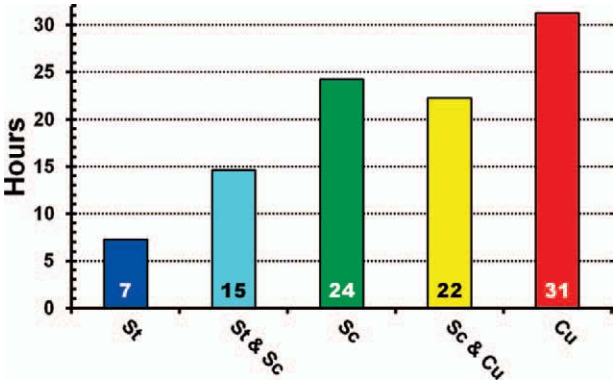

Fig. 4. RACORO flight hour distributions per cloud type. Total flight hours are plotted per cloud type sampled (or of their combinations): stratus (denoted as St), stratocumulus (denoted as Sc), and cumulus (denoted as Cu). At the base of each column, the time is expressed as a percentage of the 103 h of total cloud sampling (the percentages sum to 99% due to rounding). The cloud-type classifications are general, based on visual inspection of flight images and pilot reports.

when using common two-channel MWRs.[1] The root-mean-square (RMS) uncertainty in these MWR LWP measurements is 20–30 g m^{-2} (Westwater et al. 2001; Marchand et al. 2003; Crewell and Löhnert 2003), which is at least 20%–30% of the LWP in CLOWD systems (Turner et al. 2007b). This uncertainty appears in Fig. 6 as a tail of negative LWP that extends from 0 to −40 g m^{-2}, which accounts for almost 20% of the cumulative frequency distribution. Although this RMS uncertainty is clearly manifested as nonphysical negative values when cloud LWP is near zero, this (instantaneous) uncertainty is present for all LWPs.

[1] MWRs that are commonly used measure sky brightness temperatures at 23.8 and 31.4 GHz, from which cloud LWP and the column precipitable water vapor amount can be retrieved (e.g., Liljegren et al. 2001).

WHEN AND WHERE TO FLY

The decisions on flight time and flight pattern are critical to the goal of obtaining a good statistical sample of cloud conditions. Flight timing was determined using daily weather briefings that discussed medium-range and short-range forecasts and, on flight days, nowcasts for a final flight go/no-go decision. The briefings were held via telecon, during which graphics from forecast model output and observations were shared over the Internet using Microsoft Live Meeting. Forecast model profiles of moisture and temperature from the Global Forecast System (GFS) and North American Mesoscale Model (NAM) were visualized using BUFKIT. (BUFKIT is a forecast profile visualization and analysis tool kit; see www.wdtb.noaa.gov/tools/BUFKIT). Interpretation of these data was guided by our forecasters' intuition and knowledge of the local meteorology. Days were sought that were forecast to have large amounts of low-level moisture or cloud and without widespread (frontal) precipitation or subzero temperatures (i.e., that would cause aircraft icing). The SGP was the primary target region but, if clouds would be absent, other regions within our flight radius were considered. Medium-range forecasts (about 2–7 days) were used to schedule downtimes needed for pilot rest and instrument maintenance. Short-range forecasts (<24 h) were made before a potential flight day, using the morning update of the NAM, to assess if a flight should be scheduled and, if so, the optimal takeoff time. This time aimed to have the aircraft's 3.5-h sampling window on site during the peak probability of low-cloud occurrence. A nowcast was made 3 h before scheduled takeoff to make a go/no-go decision based on the last NAM update and real-time data [satellite imagery, aviation routine weather reports (METARs), and SGP data]. No-go criteria included bad weather conditions (presence of icing conditions, widespread precipitation, or severe weather) or unfavorable cloud conditions (forecasted low-level cloud cover either <10% or at altitudes that could not be sampled by the aircraft: i.e., cloud base <450 m or the majority of low-cloud-top heights >~3 km). The takeoff time was sometimes delayed by a couple of hours if that timing seemed more favorable for the development of clouds. Sometimes clouds did not develop when forecast or they dissipated close to the arrival time of the aircraft so, when a cloud flight was a go, a noncloud flight objective was also selected as a backup.

Flight patterns were selected from a predetermined set to meet the science objectives relevant for that day. Using the same patterns simplified flight planning and helped ensure comparable statistical sampling among flights. The standard cloud flight pattern consisted of spiral ascents plus level legs at different altitudes. The spirals gave cloud profiles over the SGP site, and the level legs provided a sampling across the cloud field and provided the level-flight data needed for turbulence and radiation observations. The level legs were flown in a triangular pattern; a 30–40-km leg was oriented along the prevailing westerlies over the SGP site, and a perpendicular leg of the same length gave statistics both in the along-wind and crosswind directions (see Fig. SB1). The hypotenuse provided a sampling independent of any potential cloud organization relative to the wind. The triangles were flown at multiple levels through cloud, below cloud base, and above cloud top to obtain boundary conditions (for details on how the flight pattern was designed to obtain the sampling needed to meet the different specific objectives, as well as other sampling patterns used, see the science and operations plan at www.arm.gov/publications/programdocs/doe-sc-arm-0806.pdf?id=60). This pattern could be adjusted at pilot's discretion if conditions warranted (e.g., if the cloud system was quickly evolving).

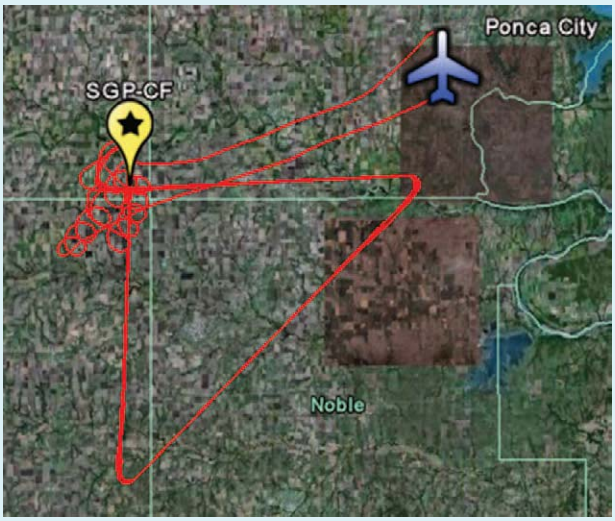

Fig. SB1. Example of a cloud flight pattern flown out of the Ponca City airport. The horizontal legs are 32 km long, and two spiral ascents were flown over the SGP.

A broad view of the aircraft measurements provides a separate perspective on how often clouds with low LWCs are present. Figure 7 gives the frequency distribution of LWC measured by the Cloud and Aerosol Spectrometer (CAS) during RACORO.[2] The frequency distribution is heavily skewed towards small LWCs, with a mode of approximately 0.01 g m^{-3} (the lowest LWC bin) and a median of 0.09 g m^{-3}. To relate these measurements to the MWR observations, vertical lines indicate values of LWC and cloud thickness that yield an LWP of 30 g m^{-2}, the approximate uncertainty of the MWR. The portion of the distribution to the left of each line is below the MWR uncertainty for the given cloud thickness. Because cloud thicknesses during RACORO were typically between 200 and 500 m, this figure suggests that 35%–70% of the clouds sampled could be below this limit and therefore problematic to measure accurately using two-channel (23 and 31 GHz) MWRs.[3]

The consistency of the aircraft LWCs and the surface-based MWR LWPs is demonstrated in Fig. 8. The MWR LWP frequency

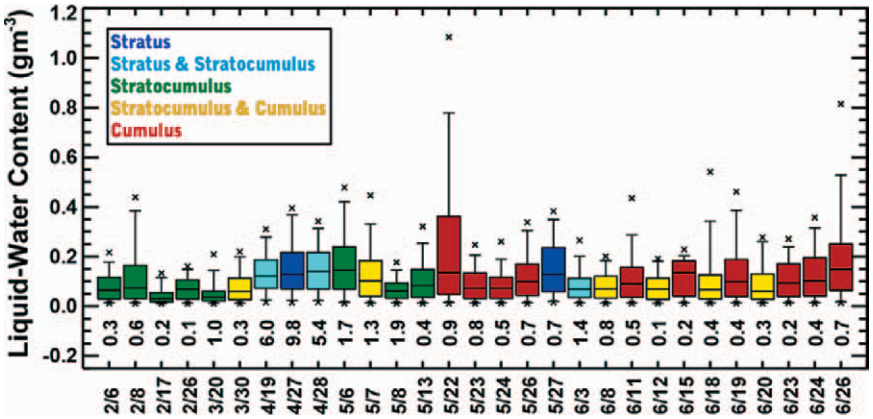

Fig. 5. RACORO LWC. Summary statistics for all RACORO cloud flights are given for LWC measured by the CAS. Box-and-whisker percentiles are as in Fig. 3, and box shading indicates the approximate cloud type encountered as explained in the legend. Cloud LWC had to be greater than 0.01 g m^{-3} for a 1-Hz sample to be included, and LWC had to meet this criterion for more than 100 s per flight for the day to be plotted. The number below each box and whisker is the number of LWC samples in thousands.

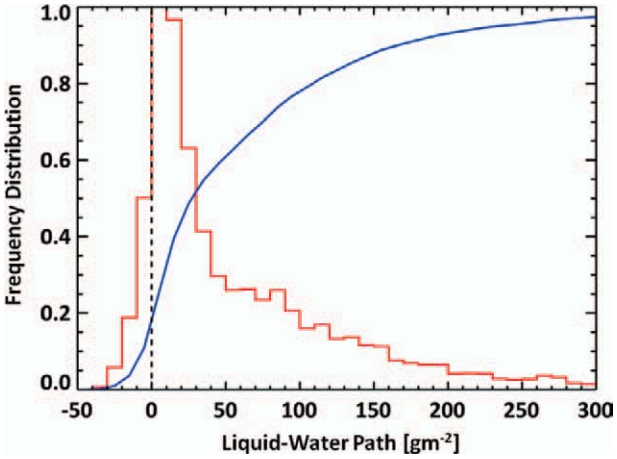

Fig. 6. Frequency distribution of RACORO LWPs. The normalized frequency distribution (red) and cumulative frequency distribution (blue) are based on MWR LWPs during RACORO when the aircraft was sampling around the SGP. The MWR dataset had biases removed from the 31.4-GHz brightness temperature so that the mean LWP under clear skies is zero (Turner et al. 2007a), although the RMS uncertainty is still 20–30 g m^{-2}. Cloud-base heights are <3 km as determined by the Active Remotely Sensed Clouds Locations (ARSCL) dataset, which determines cloud boundaries from surface lidar and radar data (Clothiaux et al. 2000). To further ensure that no clear-sky points are included, measurements were excluded when the MWR viewed a homogenous sky (indicative of clear skies), which was identified when the standard deviation of the 31-GHz brightness temperature over a 15-min window was <0.3 K.

[2] The CAS data were averaged into 200-m segments to match the averaging distance of each MWR observation, given that the MWR averaging time is 20 s and the average cloud advection speed was ~10 m s^{-1} (based on all aircraft observations of wind speed at cloud altitude). This is also approximately the distance needed to obtain a statistically significant sample of cloud particles. The length averaging includes all LWC values (including any clear-air LWC = 0 values) to represent the cloud variability within a MWR observation, and the final length-averaged LWC must be ≥0.01 g m^{-3} to be included as a cloud sample. To relate the length-averaged LWC to the LWP measured by the MWR, it must be multiplied by a representative cloud thickness.

[3] ARM MWRs recently added a channel at 90 GHz that decreases the LWP uncertainty to about 15 g m^{-2} (e.g., Crewell and Löhnert 2003).

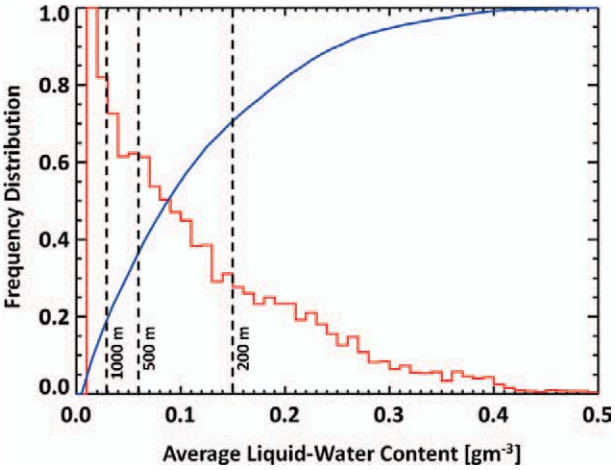

Fig. 7. Frequency distribution of RACORO LWCs. The normalized frequency distribution (red) and cumulative frequency distribution (blue) are based on all LWCs measured by the CAS during RACORO. To approximate the sampling by the MWR, CAS LWCs are averaged over 200 m (see text) and the averaged LWC had to exceed 0.01 g m^{-3} for a sample to be included. Vertical dashed lines indicate the LWCs that pertain to a 30 g m^{-2} MWR LWP uncertainty for cloud thicknesses of 1000, 500, and 200 m. The portion of the distribution to the left of a given line is below the MWR uncertainty. The widths of the LWC bins are 0.01 g m^{-3}.

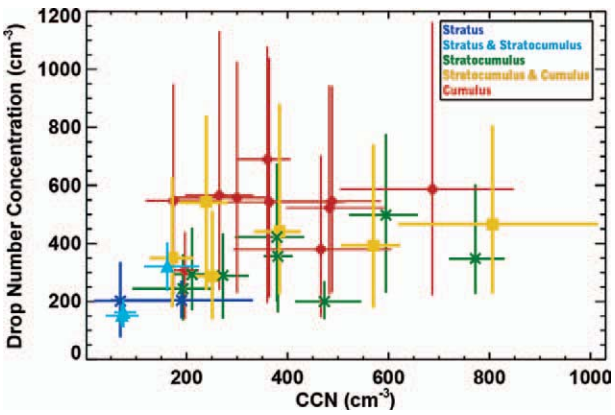

Fig. 9. Cloud drop number concentration and CCN. The relationship between cloud drop number concentration and CCN (at 0.2% SS) is given for all RACORO cloud flights. Each point represents the full flight of data when CAS LWC > 0.01 g m^{-3}. The cloud drop number concentration is from the CAS for drop diameters 2.3–34.3 μm. The point represents the median value, and the bar extends from the 25th to the 75th percentiles. Color coding (in legend) is as in Fig. 5. CCN used in this comparison are from a fixed 0.2% SS because such data are available at 1-Hz resolution and hence provide the best temporal coverage. The constant SS of 0.2% was used to represent low-LWC clouds (CLOWDs) associated with weak convection, but note that clouds with SSs greater than 0.2% would have had more CCN activated than shown here.

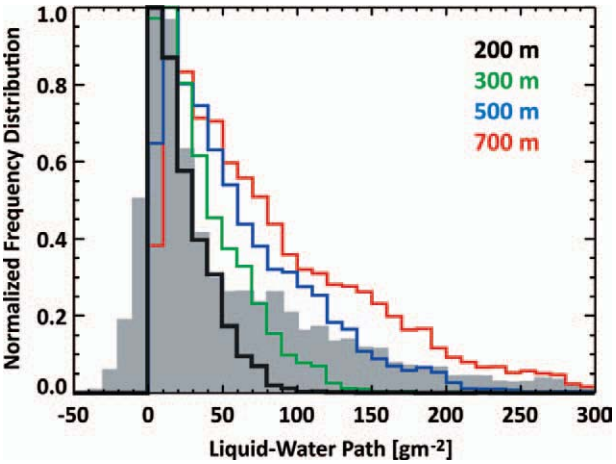

Fig. 8. Consistency of MWR LWP with LWP distributions computed from RACORO LWCs. The frequency distribution of the MWR LWP during RACORO from Fig. 6, given by the shaded area, is overlaid by LWP distributions computed from the RACORO LWC distribution from Fig. 7 (that were compiled from aircraft observations) using assumed cloud thicknesses of 200, 300, 500, and 700 m. Color coding for cloud thicknesses is given in the legend.

distribution from Fig. 6 is shown with LWP distributions computed from the LWC distribution in Fig. 7 for assumed cloud thicknesses of 200, 300, 500, and 700 m. For adiabatic growth, LWC increases linearly with height above cloud base at a rate dependent on cloud-base temperature. Assuming a random sampling with depth in cloud, the larger LWCs are expected for thicker clouds. Thus, the MWR LWP distribution should be approximated at larger LWPs by larger cloud thickness. This is confirmed by Fig. 8, where the MWR LWP distribution from 0 to 50 g m^{-2} is approximated by a 200-m-thick cloud, from 70 to 80 g m^{-2} by 300 m, from 140 to 200 g m^{-2} by 500 m, and from 260 to 280 g m^{-2} by 700 m. Further work will examine these distributions as a function of cloud thickness obtained from the SGP instruments and their variations with cloud type.

We note that these relatively small cloud thicknesses (200–500 m) complicate the derivation of vertical profiles of cloud properties from these data. The characteristics of the boundary layer and the clouds therein are linked to atmospheric motions that are driven by surface fluxes of sensible heat and moisture that vary diurnally and as a function of land surface type (e.g., Weaver and Avissar 2001). The boundary layer height for a given day was typically between ~0.5 and 2 km above ground level (not shown); however, the pilots often observed changes in cloud-base height during a flight. Because cloud thickness was only ~200–500 m,

even a slight variation (temporally or spatially) in cloud-base height will complicate the derivation of vertical profiles from the in situ data.

Aerosol–cloud relationships. Figure 9 shows that RACORO sampled a wide range of cloud and aerosol conditions. (See the "Activating aerosol" sidebar for a description of how RACORO aerosol observations can be related to CCN.) The flight medians of cloud drop number concentration N_d range from about 150 to 700 cm^{-3}, whereas the CCN number concentration medians [at 0.2% supersaturation (SS)] range from about 75 to 800 cm^{-3}. These ranges are representative of N_d in continental clouds (Miles et al. 2000) and of CCN concentrations in nonpristine environments (Hudson and Yum 2002). Figure 9 also suggests a

ACTIVATING AEROSOL

Cloud condensation nuclei (CCN) are the aerosol particles that activate (nucleate a cloud drop) at a given supersaturation (SS). The dry diameter of the smallest aerosol particle that activates at a given SS is defined here as the aerosol activation diameter. This diameter is dictated by the particle's solubility, which is governed by its chemical composition: the more soluble the particle, the smaller the activation diameter. Thus, the activation diameter provides the means for inferring the CCN composition, which is used here to compare the CCN activity aloft to that at the surface. This comparison is the first step in assessing the extent to which the long-term record of surface aerosol properties at the SGP can be combined with surface remote sensing data (e.g., updraft velocity) to estimate CCN at cloud base (Ghan et al. 2006) or predict N_d (e.g., McComiskey et al. 2009).

The aerosol activation diameter is determined by comparing the CCN concentration (at 0.2% SS) to the aerosol number size distribution, which is measured by a Differential Mobility Analyzer (DMA) in bins from 0.012 to 0.6 μm in diameter. The DMA concentrations are summed from the largest to smallest bin, and the activation diameter is the diameter of the bin where the summation yields the CCN concentration. Figure SB2a shows an example of the activation diameter calculated for the 18 March flight. For most of the flight, the value is approximately 0.15 μm; however, there are three distinct spikes in activation diameter associated with significant changes in the aerosol size distribution. These changes occur in the southwestern quadrant of the flight pattern where the pilot noted that the Twin Otter was in close proximity to several controlled burns but did not fly directly through the smoke plume. Thus, they might have flown through part of the smoke plume that was not visible to the eye but was detected by the aerosol instruments.

Figure SB2b presents activation diameter statistics that are computed for three cases: for the surface measurements for the RACORO period, for all of the aircraft data, and for the subset of the aircraft data that were above cloud. There is a notable decrease in activation diameter from the surface to above cloud. The median activation diameter at 0.2% SS for all flights was 0.14 μm; if all particles were composed of a mixture of ammonium sulfate and insoluble material, this activation diameter corresponds to an insoluble fraction of 80% (by volume). The 5th–95th percentile range of activation diameter of 0.11–0.18 μm yields insoluble fractions of 50%–90% if the remainder was ammonium sulfate. Although aerosol composition was not measured on the RACORO flights, the activation diameter analysis suggests that insoluble material composed a large fraction of the particles and that the insoluble fraction decreased with increasing altitude.

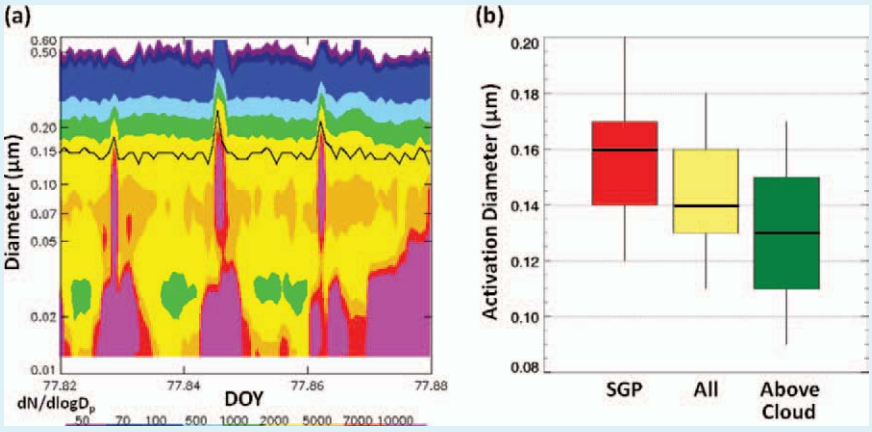

Fig. SB2. Aerosol activation diameter. The activation diameter was computed for each flight and from the SGP surface data for 0.2% SS where, for these calculations, all particles are assumed to have the same composition. (a) Example of a time series of the activation diameter calculated for part of the 18 March flight that was flown 150 m over the SGP site, where the DMA aerosol size distribution (color) is overlaid by the calculated activation diameter (black line). (b) Variability of the calculated activation diameter statistics for three cases: "SGP," for the calculation using surface instrumentation at the SGP site; "All," that includes the entire RACORO Twin Otter dataset; and "Above Cloud," for only the above-cloud legs within the aircraft dataset. The percentiles depicted in the box-and-whisker plots are 5th, 25th, 50th, 75th, and 95th.

somewhat systematic change in cloud type across this CCN–N_d phase space, where the lower N_d and CCN values coincide with the stratus cases and the upper range of these values coincide with the cumulus cases.

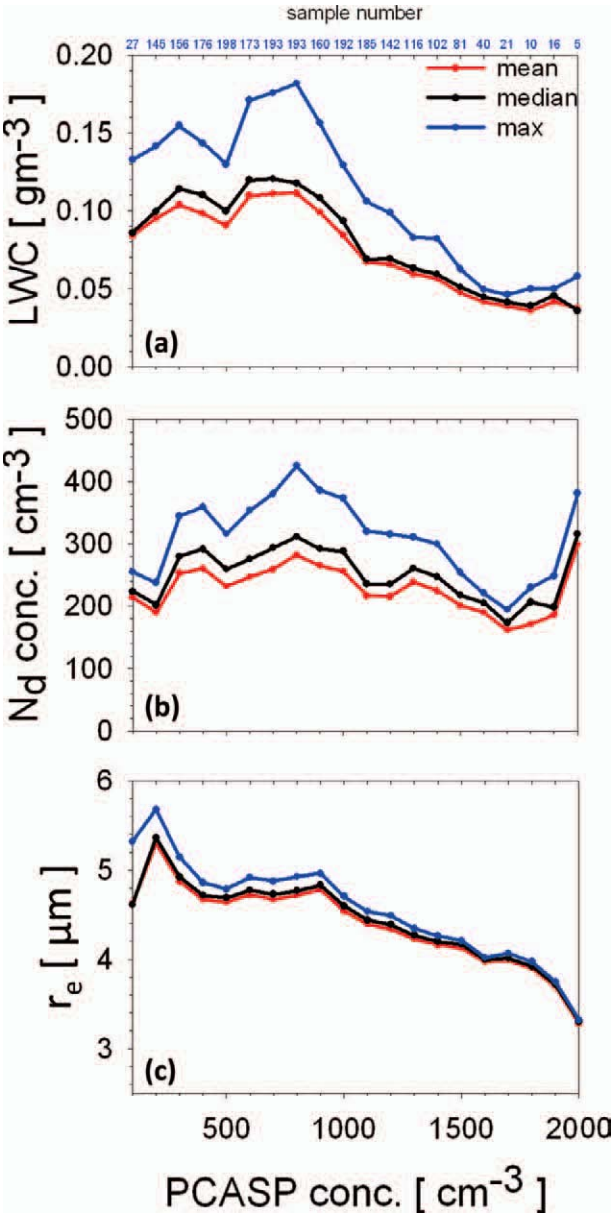

Fig. 10. Shallow, broken-cloud properties as a function of aerosol concentration. Mean, median, and maximum cloud properties for (a) LWC, (b) N_d, and (c) r_e as a function of aerosol concentration measured by the PCASP [legend given in (a)]. Values are computed for bins that are 100 cm^{-3} wide and are based on data acquired in 2,331 penetrations through shallow, broken clouds during RACORO (primarily shallow cumuli).

Because CCN concentrations varied for different cloud types, aerosol–cloud property relationships should be examined for different cloud types separately. Figure 10 shows statistics that are based on data acquired in 2,331 penetrations through shallow, broken clouds during RACORO (primarily shallow cumuli). Cloud properties, which include the mean, median, and maximum of LWC, N_d, and cloud drop effective radius r_e (Hansen and Travis 1974) are binned by aerosol concentrations measured between clouds by the Passive Cavity Aerosol Spectrometer Probe (PCASP). The PCASP measures over the diameter range 0.1–3 μm, which under weak turbulence includes most particles responsible for cloud droplet formation. Figure 10 shows lower LWC associated with higher PCASP concentration. Further, N_d does not have a strong dependence on PCASP concentration, suggesting other confounding factors are at play. Additional analysis showed that smaller updraft velocities were more prevalent for higher PCASP concentrations, consistent with clouds with lower LWC, and explaining why the same number of cloud droplets might be nucleated with higher aerosol concentrations. The observed decrease in r_e is consistent with both an increase in PCASP concentration and a decrease in LWC. Further work is examining the relationship between the less-vigorous convection and possibly enhanced entrainment and the reduced LWC for the higher amounts of aerosol loading (e.g., Lu et al. 2008).

Cloud radiative impacts. Radiometers were flown to characterize the radiative fields of the clouds and to map the time-varying spectral surface albedo around the SGP.[4] Downwelling shortwave irradiance measurements need a level orientation to be used in such energy-balance applications, but aircraft pitch or roll alters the orientation of the sensor to the direct solar beam (when present) and causes artificial variations in the downwelling irradiance. For example, broadband shortwave irradiances with tilts of 5° can exhibit errors as large as 100 W m^{-2} (Long et al. 2010). Actively stabilized platforms (e.g., Wendisch et al. 2001; Bucholtz et al. 2008) greatly decrease the measurement uncertainties due to aircraft attitude; however, these custom-made systems are still an emerging technology and are complex and difficult

[4] Surface albedo is needed to determine the amount of shortwave radiation absorbed at the surface (e.g., Li et al. 2002) and to interpret satellite observations that are affected by surface reflection. Because the SGP is surrounded by farmland, the albedo of each square of the "checkerboard" depends on the crop planted (or left barren) each year, and their values can change rapidly in May as fields undergo rapid "greening" (McFarlane et al. 2011).

to maintain and thus currently not practical for a long-term campaign such as RACORO. Instead, a new technique was developed during RACORO that corrects for tilt (Long et al. 2010), using the partitioning between direct and diffuse components measured by a newly available commercial radiometer, the Sunshine Pyranometer (SPN1). When applied to broadband data, the technique corrects for tilt up to ±10°, with 90% of the data corrected to within 10 W m^{-2} under clear skies (Long et al. 2010). This correction was applied to the RACORO downwelling broadband and narrowband shortwave irradiance data, making them suitable for energy-balance studies. This is an example of how a fast-response measurement (SPN1) can be used to characterize a slower-response measurement (Kipp and Zonen pyranometer).

An example of the radiometric data is shown in Fig. 11 for a cumulus field, where measurements were made from upward-facing radiometers flown just below cloud base. The variability of the cloud field is more evident in the broadband shortwave irradiances than in the longwave irradiances (Figs. 11a,b), due to the overhead obscuration of sun by cloud as the cumulus field is traversed. Although the diffuse longwave irradiance changes more gradually (Fig. 11b), the fast-response, narrow-field-of-view radiance measurement by the infrared thermometer (IRT) reveals a more variable structure that underlies the hemispheric-view variations.

Below-cloud radiance measurements can be used to retrieve cloud optical depth. Figure 11c shows an example where cloud optical depth was retrieved for broken-cloud fields over vegetated surfaces using radiances at 440 and 780 nm (Marshak et al. 2004; Chiu et al. 2006, 2010). Such retrievals enable mapping the horizontal variations in cloud optical depth, which can

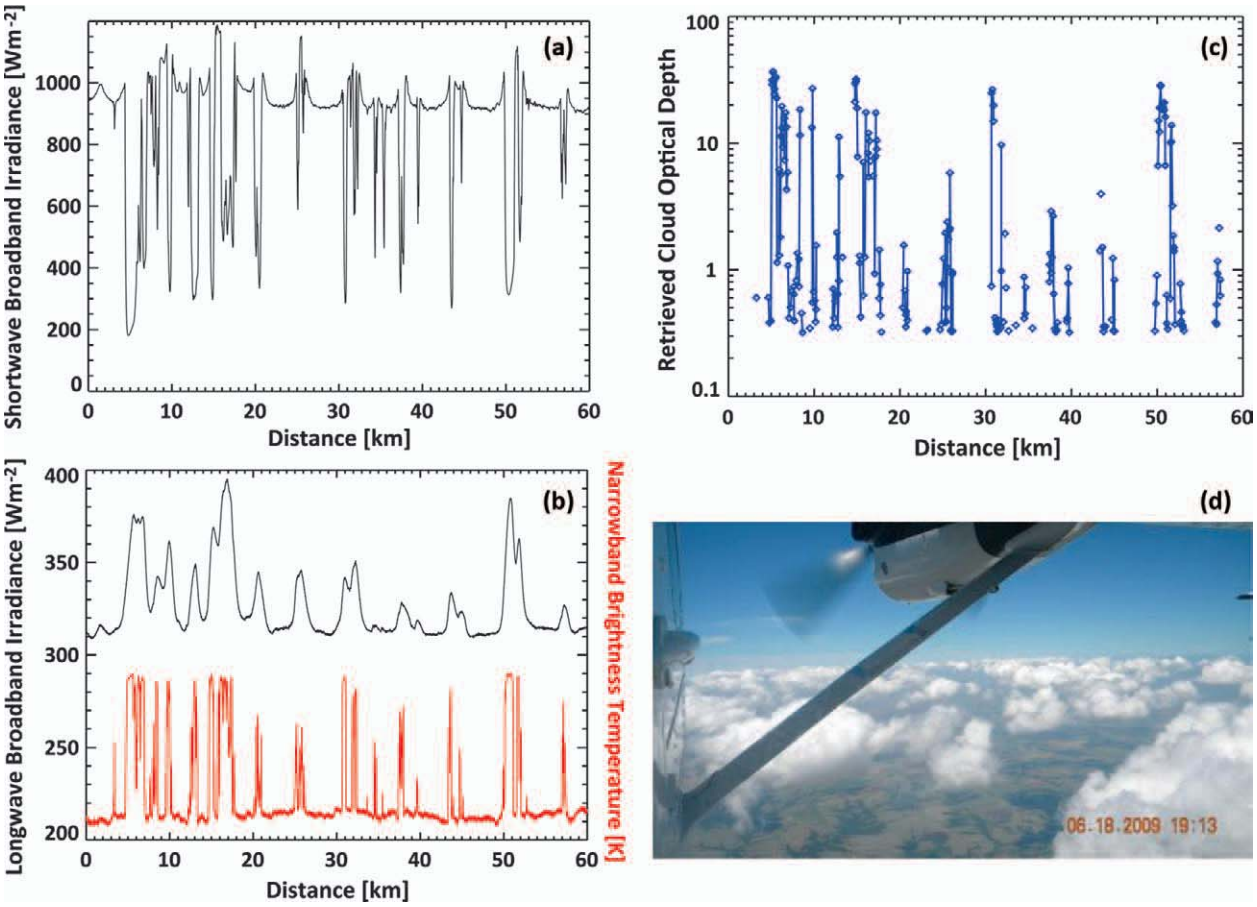

Fig 11. Cumulus field radiative impact. Examples of the radiative fields measured for a cumulus cloud field on 18 Jun. Measurements were made just below cloud base by upward-facing radiometers. (a) Downwelling broadband shortwave irradiances, adjusted to level attitude using the Long et al. (2010) tilt-correction method. (b) Downwelling broadband longwave irradiances (black) and narrowband (9.6–11.5 μm) brightness temperatures (red). Data in (a) and (b) were stored at 10 Hz, although the broadband measurements reach 95% response in 5 s. (c) Cloud optical depth retrieved using below-cloud spectral radiances at 440 and 780 nm (Marshak et al. 2004; Chiu et al. 2006, 2010). (d) Above-cloud image of the cloud field.

be used to characterize cloud subgrid-scale heterogeneity and its impact on the radiative energy budget.

Retrieval evaluation. Because RACORO operated over five months, the in situ data may be used for evaluating retrieval algorithms under a variety of conditions. The extensive set of surface measurements at the SGP enables evaluation of a broad range of retrieval algorithms, for which any refinements can benefit the site's long-term data record.

The Mixed-phase Cloud Retrieval Algorithm (MIXCRA; Turner 2007) uses ground-based observations of infrared spectral radiances to retrieve cloud LWP and r_e and can be applied to the purely liquid clouds sampled during RACORO. Its retrievals of r_e are evaluated using CAS probe data from 19 April for a single-layered cloud field composed of stratus and stratocumulus. The histograms of r_e in Fig. 12 show that MIXCRA captures the primary mode from 3 to 6 μm; however, it also suggests a secondary mode around 8 μm that is not seen in the aircraft data. The reason for this difference is under further investigation.

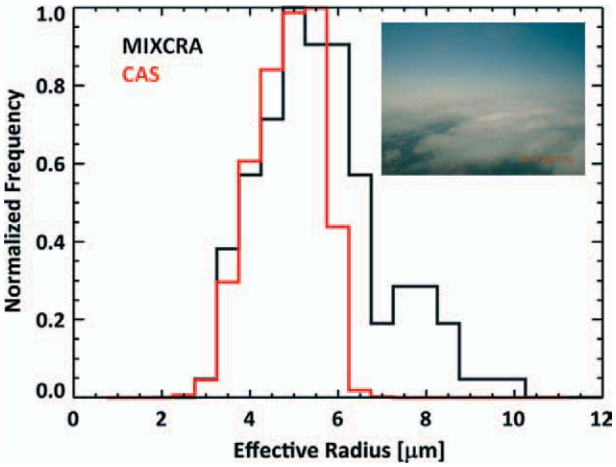

Fig. 12. Cloud property retrieval evaluation. A test of a ground-based cloud retrieval is given that uses RACORO data obtained on 19 Apr for a single-layered cloud field composed of stratus and stratocumulus (see inset image). The drop size distributions measured by the CAS are used to test the retrievals of effective radius r_e obtained from MIXCRA (Turner 2007) for the cloud field from 1400 to 1930 UTC. The method can retrieve column-average r_e when LWP $\leq$ ~50 g m^{-2}. Normalized frequency distributions of r_e are given for the MIXCRA retrievals (black) and CAS data (red). The mean and standard deviations of the distributions are 5.3 ± 1.6 μm (MIXCRA) and 4.9 ± 0.7 μm (CAS). MIXCRA uses infrared spectral radiances measured by the Atmospheric Emitted Radiance Interferometer (AERI) that has a 1.3° field of view, which yields a 17-m footprint at cloud-base height for this case. Because the AERI averaging time is 15 s and the cloud advection speed was about 17 m s^{-1} (based on aircraft observations of wind speed at cloud altitude), each MIXCRA retrieval represents an average over about 250 m of cloud. The CAS data were averaged into 250-m segments to match this averaging distance, which is also approximately the distance needed to obtain a statistically significant sample of cloud particles.

Another type of retrieval derives turbulence profiles from the SGP Raman lidar data (Wulfmeyer et al. 2010) that are needed for evaluating boundary layer parameterizations. The retrieval was tested using noncloud RACORO data from the "turbulence flights," when long, level legs were flown at different altitudes within the boundary layer. The retrieval uses water vapor mixing ratio as a tracer for turbulent motion given that, at the top of a well-mixed boundary layer, moist plumes rise from below while dry tongues descend from the free troposphere above. Aircraft observations of water vapor mixing ratio at 100 Hz from the Diode Laser Hygrometer (DLH) are used to assess the retrieval's ability to measure the statistics of this turbulent mixing (e.g., its variance). Figure 13 shows a comparison between the retrieval and DLH data for the 31 May flight. To be successful, the retrieval must separate the contributions to the total variance that comes from the atmosphere and from instrumental noise. This case provides an excellent example of how the retrieved atmospheric water vapor variance matches the aircraft observations to within the uncertainties at all but one level, clearly supporting the retrieval method.[5] Further tests are planned using other clear-sky cases, before applying the technique to the more challenging problem of determining sub-cloud turbulence.

SUMMARY. The 2009 RACORO campaign obtained extended-term, in situ characterizations of boundary layer cloud fields needed to investigate cloud processes and evaluate and refine existing retrieval algorithms (e.g., Table 1). The observations provide a multidisciplinary dataset for open use by the atmospheric sciences community. Our review of these observations suggests that the dataset is rich and that the five-month period covers a range of environmental conditions during the seasonal changes from winter to summer. These data, which

[5] The agreement also confirms the applicability of the Taylor's hypothesis (i.e., frozen turbulence) assumed in the turbulence retrieval, provided there are not compensating errors.

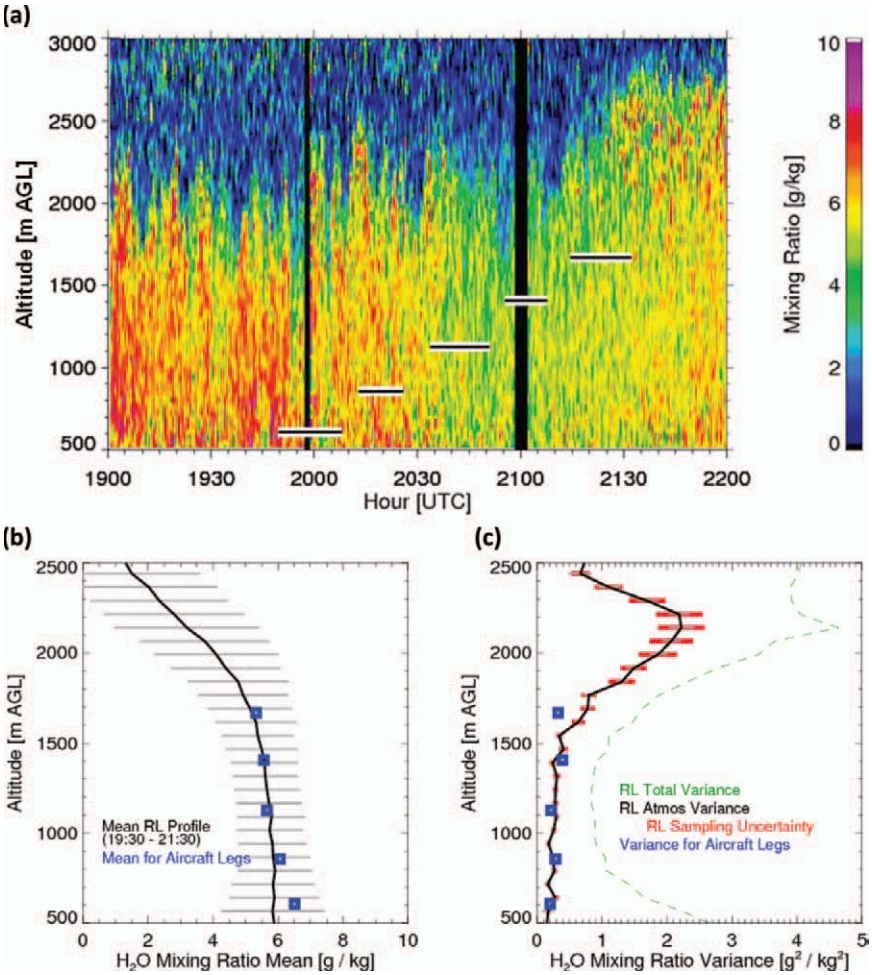

Fig. 13. Turbulence retrieval evaluation. (a) Time–height cross section of water vapor mixing ratio measured by the Raman lidar on 31 May (with 10-s temporal and 75-m vertical resolution), with the Twin Otter flight legs superimposed (horizontal black lines). Profiles of the water vapor mixing ratio (b) mean and (c) variance are given for the Raman lidar and aircraft DLH measurements for the 2-h period from 1930 to 2130 UTC. The Raman lidar analysis needs to separate the contribution to the total variance (green dashed line) that comes from instrumental noise versus that from the atmosphere (black line). The analysis requires a good signal to noise ratio in the Raman Lidar data and a more or less stationary (nongrowing) boundary layer when the aircraft was above the SGP facility.

are augmented by the suite of surface-based observations available from the SGP ACRF site, enable interdisciplinary studies that are not possible with shorter-term deployments. All RACORO data are freely available, after registration, online (at www.arm.gov/campaigns/aaf2009racoro#data).

ACKNOWLEDGMENTS. We gratefully acknowledge the many contributions by Debbie Ronfeld (AAF logistics point of contact), pilots Mike Hubbell and Chris McGuire, copilot Dave McSwaggan, Jesse Barge (cabin instrument operations), and Greg Cooper (CIRPAS aircraft operations) and the web and media support by Sherman Beus and Lynne Roeder, respectively. We are delighted to acknowledge the NASA King Air team for their collaborative participation and excellent flight coordination (PIs Rich Ferrare, Chris Hostetler, and Brian Cairns). Data used in this article are from the U.S. Department of Energy AAF RACORO campaign and from the SGP ARM Climate Research Facility. This research was supported by the U.S. Department of Energy's Atmospheric Science Program Atmospheric System Research, an Office of Science, Office of Biological and Environmental Research program, under the following grants/contracts: DE-AC02-98CH10886 and the Earth System Modeling Program via the FASTER Project (AMV, TT); DE-SC0005008 (JAO, EA); DE-FG02-08ER64538 (DDT); DE-FG02-02ER63337 (GM, HJY); DE-FG02-07ER64378 (GM, HJY); DE-FG02-09ER64770 (GM, HJY); DE-SC0001279 (GM, HJY); DE-SC0005507 (GM, HJY); DE-SC0002037 (GF); DE-AC06-76RLO 1,830 (CNL, SAM); DE-FG02-05ER64062 (DH, JWM); DE-AI05-09OR23371 (AB); DE-SC0000543 (GSD); DE-AI02-08ER64562 (AM); DE-FG02-08ER64563 (AM, JCC); and DE-FG02-08ER54564 (AM).

REFERENCES

Ackerman, T. P., and G. M. Stokes, 2003: The Atmospheric Radiation Measurement Program. *Phys. Today,* **56**, 38–45, doi:10.1063/1.1554135.

Albrecht, B., 1989: Aerosols, cloud microphysics and fractional cloudiness. *Science,* **245,** 1227–1230.

Andrews, E., P. J. Sheridan, J. A. Ogren, and R. Ferrare, 2004: In situ aerosol profiles over the southern great

plains cloud and radiation test bed site: 1. Aerosol optical properties. *J. Geophys. Res.,* **109**, D06208, doi:10.1029/2003JD004025.

Berg, L. K., C. M. Berkowitz, J. C. Barnard, G. Senum, and S. R. Springston, 2011: Observations of the first aerosol indirect effect in shallow cumuli. *Geophys. Res. Lett.,* **38,** L03809, doi:10.1029/2010GL046047.

Betts, A. K., and C. Jakob, 2002: Evaluation of the diurnal cycle of precipitation, surface thermodynamics, and surface fluxes in the ECMWF model using LBA data. *J. Geophys. Res.,* **107,** 8045, doi:10.1029/2001JD000427.

Boers, R., and R. M. Mitchell, 1994: Absorption feedback in stratocumulus clouds: Influence on cloud top albedo. *Tellus,* **46A,** 229–241.

Bony, S., and J.-L. Dufresne, 2005: Marine boundary layer clouds at the heart of tropical cloud feedback uncertainties in climate models. *Geophys. Res. Lett.,* **32,** L20806, doi:10.1029/2005GL023851.

Brown, A. R., and Coauthors, 2002: Large-eddy simulation of the diurnal cycle of shallow cumulus convection. *Quart. J. Roy. Meteor. Soc.,* **128,** 1075–1093.

Bucholtz, A., R. T. Bluth, B. Kelly, S. Taylor, K. Batson, A. W. Sarto, and T. P. Toonman, and R. F. McCoy Jr., 2008: The Stabilized Radiometer Platform (STRAP)—An actively stabilized horizontally level platform for improved aircraft irradiance measurements. *J. Atmos. Oceanic Technol.,* **25,** 2161–2175.

Cahalan, R. F., and J. H. Joseph, 1989: Fractal statistics of cloud fields. *Mon. Wea. Rev.,* **117,** 261–272.

Cairns, B., F. Waquet, K. Knobelspiesse, J. Chowdhary, and J. L. Deuzé, 2009: Polarimetric remote sensing of aerosols over land surfaces. *Satellite Aerosol Remote Sensing over Land,* A. A. Kokhanovsky and G. de Leeuw, Eds., Springer, 295–325.

Chaboureau, J.-P., F. Guichard, J.-L. Redelsperger, and J.-P. Lafore, 2004: The role of stability and moisture in the diurnal cycle of convection over land. *Quart. J. Roy. Meteor. Soc.,* **130,** 3105–3117.

Charlson, R. J., A. S. Ackerman, F. A.-M. Bender, T. L. Anderson, and Z. Liu, 2007: On the climate forcing consequences of the albedo continuum between cloudy and clear air. *Tellus,* **59B,** 715–727, doi:10.1111/j.1600-0889.2007.00297.x.

Chiu, J. C., A. Marshak, Y. Knyazikhin, W. J. Wiscombe, H. W. Barker, J. C. Barnard, and Y. Luo, 2006: Remote sensing of cloud properties using ground-based measurements of zenith radiance. *J. Geophys. Res.,* **111,** D16201, doi:10.1029/2005JD006843.

——, C.-H. Huang, A. Marshak, I. Slutsker, D. M. Giles, B. N. Holben, Y. Knyazikhin, and W. J. Wiscombe, 2010: Cloud optical depth retrievals from the Aerosol Robotic Network (AERONET) cloud mode observations. *J. Geophys. Res.,* **115,** D14202, doi:10.1029/2009JD013121.

Clothiaux, E. E., T. P. Ackerman, G. G. Mace, K. P. Moran, R. T. Marchand, M. Miller, and B. E. Martner, 2000: Objective determination of cloud heights and radar reflectivities using a combination of active remote sensors at the ARM CART sites. *J. Appl. Meteor,* **39,** 645–665.

Crewell, S., and U. Löhnert, 2003: Accuracy of cloud liquid water path from ground-based microwave radiometer 2. Sensor accuracy and synergy. *Radio Sci.,* **38,** 8042, doi:10.1029/2002RS002634.

Dey, S., L. Di Girolamo, and G. Zhao, 2008: Scale effect on statistics of the macrophysical properties of trade wind cumuli over the tropical western Atlantic during RICO. *J. Geophys. Res.,* **113,** D24214, doi:10.1029/2008JD010295.

Ghan, S. J., and Coauthors, 2006: Use of in situ cloud condensation nuclei, extinction, and aerosol size distribution measurements to test a method for retrieving cloud condensation nuclei profiles from surface measurements. *J. Geophys. Res.,* **111,** D05S10, doi:10.1029/2004JD005752.

Hair, J. W., and Coauthors, 2008: Airborne high spectral resolution lidar for profiling aerosol optical properties. *Appl. Opt.,* **47,** 6734–6752, doi:10.1364/AO.47.006734.

Hansen, J. E., and L. D. Travis, 1974: Light scattering in planetary atmospheres. *Space Sci. Rev.,* **16,** 527–610.

Hartmann, D. L., M. E. Ockert-Bell, and M. L. Michelsen, 1992: The effect of cloud type on Earth's energy balance: Global analysis. *J. Climate,* **5,** 1281–1304.

Hudson, J. G., and S. S. Yum, 2002: Cloud condensation nuclei spectra and polluted and clean clouds over the Indian Ocean. *J. Geophys. Res.,* **107,** 8022, doi:10.1029/2001JD000829.

Illingworth, A. J., and Coauthors, 2007: Cloudnet: Continuous evaluation of cloud profiles in seven operational models using ground-based observations. *Bull. Amer. Meteor. Soc.,* **88,** 883–898.

IPCC 2007: *Climate Change 2007: The Physical Science Basis. Contirbution of Working Group I to the Fourth Assessment Report of the Intergovernmental Panel on Climate Change.* Cambridge University Press, 996 pp.

Khairoutdinov, M., and D. Randall, 2006: High-resolution simulation of shallow-to-deep convection transition over land. *J. Atmos. Sci.,* **63,** 3421–3436.

Koren, I., L. A. Remer, Y. J. Kaufman, Y. Rudich, and J. V. Martins, 2007: On the twilight zone between clouds and aerosols. *Geophys. Res. Lett.,* **34,** L08805, doi:10.1029/2007GL029253.

Lazarus, S. M., S. K. Krueger, and G. G. Mace, 2000: A cloud climatology of the Southern Great Plains ARM CART. *J. Climate,* **13,** 1762–1775.

Lenderink, G., and Coauthors, 2004: The diurnal cycle of shallow cumulus clouds over land: A single-column model intercomparison study. *Quart. J. Roy. Meteor. Soc.,* **130,** 3339–3364.

Li, Z., M. C. Cribb, and A. P. Trishchenko, 2002: Impact of surface inhomogeneity on solar radiative transfer under overcast conditions. *J. Geophys. Res.,* **107,** 4294, doi:10.1029/2001JD000976.

Liljegren, J. C., E. E. Clothiaux, G. G. Mace, S. Kato, and X. Dong, 2001: A new retrieval for cloud liquid water path using a ground-based microwave radiometer and measurements of cloud temperature. *J. Geophys. Res.,* **106,** 14 485–14 500.

Long, C. N., A. Bucholtz, H. Jonsson, B. Schmid, A. M. Vogelmann, and J. Wood, 2010: A method of correcting for tilt from horizontal in downwelling shortwave irradiance measurements on moving platforms. *Open Atmos. Sci. J.,* **4,** 78–87, doi:10.2174/1874282301004010078.

Lu, M.-L., G. Feingold, H. H. Jonsson, P. Y. Chuang, H. Gates, R. C. Flagan, and J. H. Seinfeld, 2008: Aerosol-cloud relationships in continental shallow cumulus. *J. Geophys. Res.,* **113,** D15201, doi:10.1029/2007JD009354.

Marchand, R., T. P. Ackerman, E. R. Westwater, S. A. Clough, K. Cady-Pereira, and J. C. Liljegren, 2003: An assessment of microwave absorption models and retrievals of cloud liquid water using clear-sky data. *J. Geophys. Res.,* **108,** 4773, doi:10.1029/2003JD003843.

Marshak, A., A. Davis, W. Wiscombe, and R. Cahalan, 1998: Radiative effects of sub-mean free path liquid water variability observed in stratiform clouds. *J. Geophys. Res.,* **103** (D16), 19 557–19 567.

——, Y. Knyazikhin, K. D. Evans, and W. J. Wiscombe, 2004: The "RED versus NIR" plane to retrieve broken-cloud optical depth from ground-based measurements. *J. Atmos. Sci.,* **61,** 1911–1925.

——, S. Platnick, T. Várnai, G. Wen, and R. F. Cahalan, 2006: Impact of three-dimensional radiative effects on satellite retrievals of cloud droplet sizes. *J. Geophys. Res.,* **111,** D09207, doi:10.1029/2005JD006686.

McComiskey, A., G. Feingold, A. S. Frisch, D. D. Turner, M. A. Miller, J. C. Chiu, Q. Min, and J. A. Ogren, 2009: An assessment of aerosol-cloud interactions in marine stratus clouds based on surface remote sensing. *J. Geophys. Res.,* **114,** D09203, doi:10.1029/2008JD011006.

McFarlane, S. A., K. L. Gaustad, E. J. Mlawer, C. N. Long, and J. Delamere, 2011: Development of a high spectral resolution surface albedo product for the ARM Southern Great Plains central facility. *Atmos. Meas. Tech.,* **4,** 1713–1733.

McFarquhar, G. M., S. Platnick, L. Di Girolamo, H. Wang, G. Wind, and G. Zhao, 2004: Trade wind cumuli statistics in clean and polluted air over the Indian Ocean from in situ and remote sensing measurements. *Geophys. Res. Lett.,* **31,** L21105, doi:10.1029/2004GL020412.

——, B. Schmid, A. Korolev, J. A. Ogren, P. B. Russell, J. Tomlinson, D. D. Turner, and W. Wiscombe, 2011: Airborne needs for climate and atmospheric research. *Bull. Amer. Meteor. Soc.,* **92,** 1193–1196.

Miles, N. L., J. Verlinde, and E. E. Clothiaux, 2000: Cloud droplet size distributions in low-level stratiform clouds. *J. Atmos. Sci.,* **57,** 295–311.

Pincus, R., and M. B. Baker, 1994: Effect of precipitation on the albedo susceptibility of clouds in the marine boundary layer. *Nature,* **372,** 250–252, doi:10.1038/372250a0.

Rio, C., F. Hourdin, J.-Y. Grandpeix, and J.-P. Lafore, 2009: Shifting the diurnal cycle of parameterized deep convection over land. *Geophys. Res. Lett.,* **36,** L07809, doi:10.1029/2008GL036779.

Sengupta, M., E. E. Clothiaux, T. P. Ackerman, S. Kato, and Q. Min, 2003: Importance of accurate liquid water path for estimation of solar radiation in warm boundary layer clouds: An observational study. *J. Climate,* **16,** 2997–3009.

Turner, D. D., 2007: Improved ground-based liquid water path retrievals using a combined infrared and microwave approach. *J. Geophys. Res.,* **112,** D15204, doi:10.1029/2007JD008530.

——, S. A. Clough, J. C. Liljegren, E. E. Clothiaux, K. Cady-Pereira, and K. L. Gaustad, 2007a: Retrieving liquid water path and precipitable water vapor from Atmospheric Radiation Measurement (ARM) microwave radiometers. *IEEE Trans. Geosci. Remote Sens.,* **45,** 3680–3690, doi:10.1109/TGRS.2007.903703.

——, and Coauthors, 2007b: Thin liquid water clouds: Their importance and our challenge. *Bull. Amer. Meteor. Soc.,* **88,** 177–190.

Twomey, S., 1974: Pollution and the planetary albedo. *Atmos. Environ.,* **8,** 1251–1256.

Weaver, C. P., and R. Avissar, 2001: Atmospheric disturbances caused by human modification of the landscape. *Bull. Amer. Meteor. Soc.,* **82,** 269–281.

Wen, G., A. Marshak, R. F. Cahalan, L. A. Remer, and R. G. Kleidman, 2007: 3-D aerosol-cloud radiative interaction observed in collocated MODIS and ASTER images of cumulus cloud fields. *J. Geophys. Res.,* **112,** D13204, doi:10.1029/2006JD008267.

Wendisch, M., D. Müller, D. Schell, and J. Heintzenberg, 2001: An airborne spectral albedometer with active horizontal stabilization. *J. Atmos. Oceanic Technol.,* **18,** 1856–1866.

Westwater, E. R., Y. Han, M. D. Shupe, and S. Matrosov, 2001: Analysis of integrated cloud liquid and precipitable water vapor retrievals from microwave radiometers during the surface heat budget of the Arctic Ocean project. *J. Geophys. Res.,* **106,** 32 019–32 030.

Williams, K. D., and G. Tselioudis, 2007: GCM intercomparison of global cloud regimes: Present-day evaluation and climate change response. *Climate Dyn.,* **29,** 231–250, doi:10.1007/s00382-007-0232-2.

Wulfmeyer, V., S. Pal, D. D. Turner, and E. Wagner, 2010: Can water vapour Raman lidar resolve profiles of turbulent variables in the convective boundary layer? *Bound.-Layer Meteor.,* **136,** 253–284, doi:10.1007/s10546-010-9494-z.

Zhang, M. H., and Coauthors, 2005: Comparing clouds and their seasonal variations in 10 atmospheric general circulation models with satellite measurements. *J. Geophys. Res.,* **110,** D15S02, doi:10.1029/2004JD005021.